Synthesis of an Alginate-Based Fe$_3$O$_4$−MnO$_2$ Xerogel and Its Application for the Concurrent Elimination of Cr(VI) and Cd(II) from Aqueous Solution

Aditya Kumar, Satgur Prasad, Prem N. Saxena, Nasreen G. Ansari,* and Devendra K. Patel*

Read Online

ACCESS | Metrics & More | Article Recommendations | SI Supporting Information

ABSTRACT: In this study, magnetite−manganese oxide (Fe$_3$O$_4$−MnO$_2$) nanoparticles were synthesized and immobilized on alginate, producing a magnetite−manganese oxide xerogel (mMOX). This eco-friendly xerogel was used as an adsorbent of Cr(VI) and Cd(II). It was mesoporous and thermally stable, as determined by Brunauer−Emmett−Teller and thermogravimetric analysis. A scanning electron microscope coupled with an energy-dispersive X-ray system, Zetasizer, and attenuated total reflectance−Fourier transform infrared were used for characterization of adsorbents. The performance of the mMOX was investigated for the simultaneous adsorption of Cr(VI) and Cd(II) at different temperatures, pH values, contact times, initial concentrations of the adsorbate, and adsorbent doses. The developed xerogel

(mMOX) showed high adsorption capacities of 3.86 mg/g for Cr(VI) and 3.95 mg/g for Cd(II) on 120 min of contact time with 5 ppm Cr(VI) and Cd(II) solution. The kinetic data fitted well with the pseudo-second order, while the Freundlich isotherm model was found to be fit for adsorption data. Thermodynamic study revealed the adsorption to be spontaneous and exothermic. The adsorbent showed useful application for real water samples by more than 75% uptake of Cr and Cd with low adsorption of Na, K, and Mg. The regeneration study indicated that the mMOX could be reused up to six cycles with more than 50% removal of Cr(VI) and Cd(II) ions from aqueous solution with minimal leaching of metal ions (Fe, Ca, Na, K, and Mn) into the solution.
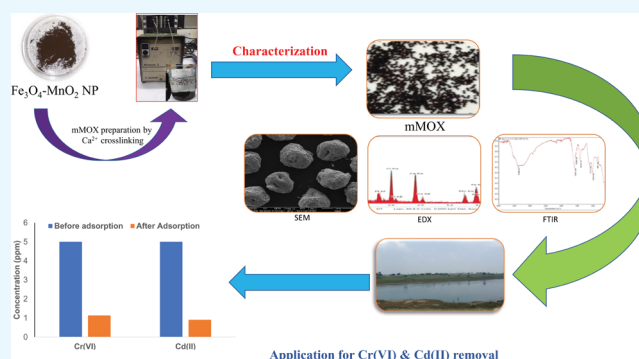
INTRODUCTION

Heavy metals are well-known water contaminants that are posing serious problems to living beings worldwide.[1] They are introduced into the environment, naturally or anthropogenically, which includes the erosion of rocks, volcanic activities, mining, and combustion of fossil fuels.[2] Their toxicity arises because of their nonbiodegradable nature, thus making them dangerous for aquatic organisms.[3] There are many heavy metals such as mercury, arsenic, chromium, lead, and cadmium that are highly toxic at low concentrations.[4] Their non-biodegradable and accumulative nature makes them more hazardous for living beings.[5] Chromium is a toxic heavy metal which, on exposure to the human body, gets absorbed and induces carcinogenesis and cytotoxicity in the form of chromate and dichromate. Textile dyeing and electroplating are some common sources of chromium generation.[6,7] Cadmium is another heavy metal that comes into the environment due to human activities such as the combustion of fossil fuels and releasing of sewage sludge into water bodies.[8] Cadmium is considered toxic since it binds to mitochondria and can inhibit cellular respiration.[9] Hence, both cadmium and chromium are highly toxic to human health in the form of Cr(VI) and Cd(II). Consumption of water contaminated by

Cr(VI) could be lethal for the kidneys and nervous system. Similarly, consuming Cd(II)-affected drinking water could induce carcinogenicity and lead to organ failures such as the lungs and kidneys.[10] In drinking water, the maximum concentration level of Cr and Cd was set as 0.1 and 0.005 ppb, respectively, by the United States Environmental Protection Agency (USEPA).[11] There are many conventional water decontamination techniques such as ion exchange, reverse osmosis, chemical precipitation, and electrolysis. However, they suffer from some drawbacks in terms of their cost and compatibility.[12] In the past few years, nanotechnology has emerged as a promising tool for removing different contaminants from wastewater and for being highly efficient and cost-effective.[13] Using the adsorption phenomenon, several nanomaterials that showed promising results in water decontamination have been developed.[14−17] Nanomaterials
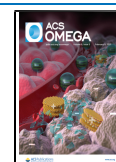
have the benefit since they provide a large surface area, which facilitates the uptake of heavy metals from their aqueous solutions. These nanomaterials can be carbon-based (carbon nanotubes and graphene oxide), metal oxide nanomaterials (magnetite and aluminum oxide), and so forth.[18]

Magnetite (Fe_3O_4) nanoparticles have gained considerable interest in the removal of heavy metal ions because of their low cost and easy separation with the aid of an external magnetic field.[19] It has been reported that Fe_3O_4 nanoparticles alone have low adsorption potential and surface area for heavy metal adsorption.[20] There is therefore a need to modify the Fe_3O_4 composite and make use of its magnetic property and stability to remove Cd and Cr ions from aqueous solution. Manganese oxide (MnO_2) nanoparticles are known to have high surface areas, and they can be used to modify Fe_3O_4 to eliminate heavy metal ions from aqueous media through adsorption or the ion exchange phenomenon.[21]

Magnetite–manganese oxide ($Fe_3O_4–MnO_2$) nanoparticles have successfully found applications in removing heavy metals from water, but their complete separation from the aqueous solution is still an issue. Due to this limitation, it is not easy to reuse, which does not allow it to be used as an effective adsorbent on a large scale.[22] However, this limitation can be overcome by coating or packing them on supporting materials.[23,24] Alginate-based supporting materials have shown positive results for the treatment of water contaminated by heavy metals.[25] Alginate is a naturally occurring polysaccharide that comprises the basic structure of the algal cell wall. They have α-L guluronic acids and β-D mannuronic acids joined together by 1,4 linkage.[26] Due to their low cost, biocompatibility, and functional groups, they have been extensively used as the supporting material for many nanoparticles. They have the property of producing thermally irreversible gels on coming in contact with polyvalent ions.[27] The gels can be classified based on their drying methods, which include air-drying (xerogel), freeze-drying (cryogel), and supercritical-drying (aerogel).[28]

No work has yet been published to the best of our understanding, which involved the alginate-supported $Fe_3O_4–MnO_2$ composite xerogel for the simultaneous removal of chromium and cadmium from their aqueous solution. In this study, $Fe_3O_4–MnO_2$ nanoparticles were synthesized and characterized and then immobilized on alginate to produce xerogel as an adsorbent. The performance of an eco-friendly xerogel was investigated at different parameters such as pH, temperature, the contact time of the adsorbent with the adsorbate, initial concentration of the adsorbate, and adsorbent dose. Adsorption and kinetic modeling have also been carried out to establish the mechanism of adsorption. The study demonstrated that the developed xerogel has good adsorption capacities for Cr(VI) and Cd(II) up to six regeneration cycles. The adsorbent has been successfully used for the adsorption of Cr(VI) and Cd(II) from real water samples also.

Synthesis of Magnetite–Manganese Oxide (mMO) Nanoparticles. Magnetite–manganese oxide (mMO) nanoparticles were produced by the coprecipitation method with minor modifications.[29] About 500 mL of 2.5 mmol of $FeSO_4$·$7H_2O$ was prepared in deionized water. Then, 2.5 mL of 5 M NaOH (5 M) was added and subjected to continuous stirring at 323 K. When the green suspension was generated, 250 ml of 2.5 mmol of $KMnO_4$ was added dropwise into the reaction solution with constant stirring at a constant temperature of 323 K, which produced a dark brown precipitate of $Fe_3O_4–MnO_2$.

The residue was separated using an external magnetic field and finally washed with ethanol and deionized water three times. The precipitate obtained was dried in a vacuum oven at 323 K to obtain $Fe_3O_4–MnO_2$ nanoparticles.

Preparation of Magnetite–Manganese Oxide-Immobilized Alginate Beads (mMO Xerogel). mMO was immobilized into alginate beads by a simple protocol in which sodium alginate (1 g) and mMO nanoparticles (0.5 g) were taken in a beaker followed by the addition of 100 mL of deionized water (Milli-Q) and mixed thoroughly using a magnetic stirrer to make a homogenous mixture. This homogeneous suspension was dropped into $CaCl_2$ solution (50 mM), carefully using a capillary automated with a peristaltic pump to form uniform $Fe_3O_4–MnO_2$ beads (due to the formation of cross-links between Ca^{2+} and carboxyl and hydroxyl groups of sodium alginate), and was immersed in $CaCl_2$ solution for 12 h. The beads were washed four to five times with deionized water to eliminate the excess of calcium ions. Finally, the beads were air-dried to form the $Fe_3O_4–MnO_2$ xerogel (mMOX). The bare alginate xerogel (AX) was also prepared to compare the mMO xerogel by the same procedure without adding mMO nanoparticles.

Characterization of Magnetite–Manganese Oxide Alginate Beads (mMO Beads). The analysis of the mMOX for its Brunauer–Emmett–Teller (BET) surface area, pore volume, and pore diameter was carried out using Quantachrome Instruments, USA. The samples were degassed for 3 h at 110 °C to remove any impurities present on the surface of the mMOX. The thermal stability of adsorbents was determined using a thermogravimetric analysis (TGA) analyzer (Mettler Toledo Stare, Columbus) with heating at a rate of 10 °C per minute from 25 to 1000 °C, under steady flow of N_2 gas. Samples of the synthesized materials were examined by field emission scanning electron microscopy (FE-SEM, QUANTA FEG 450, FEI, Netherland) coupled with an energy-dispersive X-ray (EDX) analysis system for their surface morphology and elemental composition. The surface morphology of gels was analyzed using a secondary electron detector at an accelerating voltage of 20 kV. Elemental composition of the adsorbent was determined using an EDX detector (Apollo XL, USA) attached to the scanning electron microscope. The zeta potentials at various solution pH values ranging from 2 to 12 were measured using a dynamic light scattering approach with Zetasizer Nano-ZSP equipped with a HeNe 633 nm laser (model ZEN3600; Malvern, U.K.). The attenuated total reflectance–Fourier transform infrared (ATR–FTIR) spectra of the $Fe_3O_4–MnO_2$ (mMO) nanoparticles, bare calcium AX, and $Fe_3O_4–MnO_2$ xerogels (mMOX) were obtained using a Thermo Fisher (Nicolet, iS5, USA) FT-IR instrument equipped with diamond ATR crystals with the scanning range from 400 to 4000 cm^{-1} at a rate of 32 scans/minute.

Selection of the Adsorbent. The performance of three adsorbents, viz., the AX, mMO nanoparticles, and mMOX, was checked based on their removal percentage (% R) of Cr(VI) and Cd(II), which were analyzed on an atomic absorption spectrometer (PerkinElmer, PinAAcle 900F and Analytik Jena, ZEEnit 700). In this, 10 mg dose of each adsorbent was used for adsorption study of both Cr(VI) and Cd(II) at a concentration of 5 ppm.

Quality Control for AAS. The instrument is calibrated before the analysis of metals by standard reference materials (SRMs). The calibration graph obtained after running standards had a linear correlation coefficient greater than
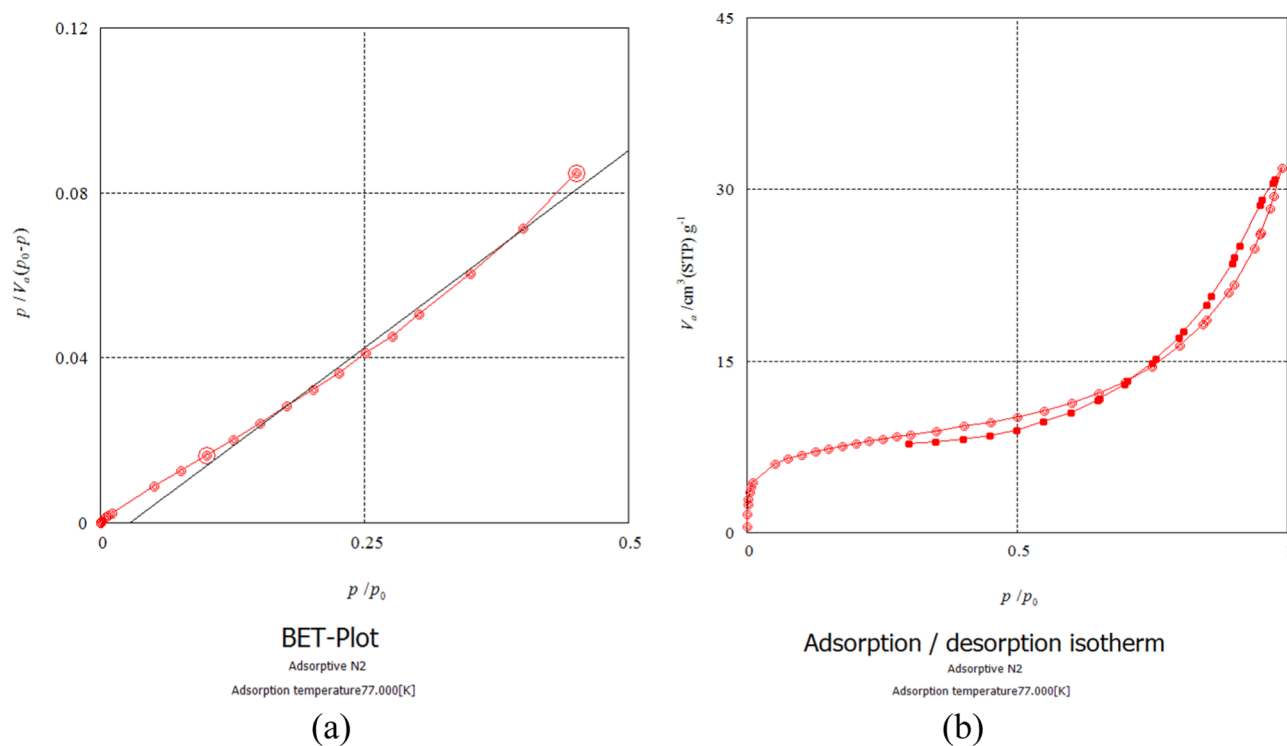
(a)   (b)

Figure 1. BET surface area analysis; (a) BET plot of N_2 adsorption. (b) BET plot of the N_2 adsorption−desorption isotherm.
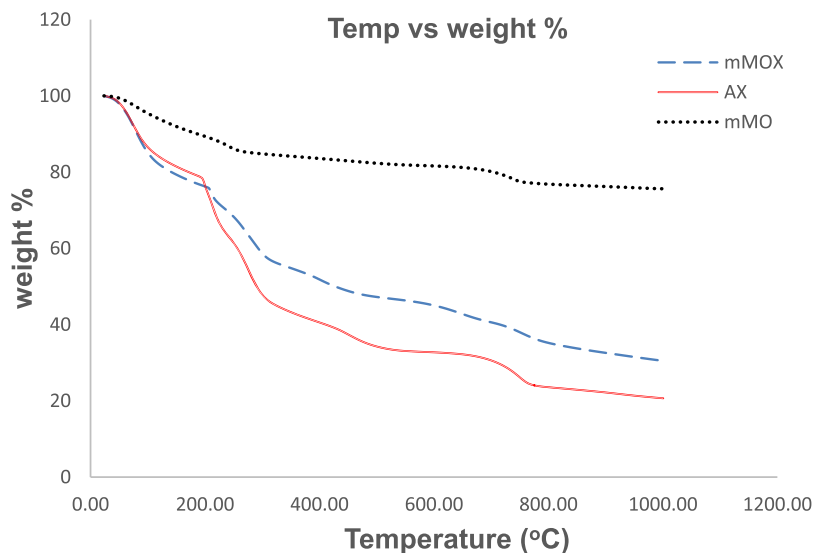

Figure 2. TGA plot of the mMOX, AX, and mMO.

0.99 ($R^2 > 0.99$). Furthermore, sample blank and reference standards were run parallel with the samples to ensure the quality of data.

Batch Adsorption Experiment. Adsorption experiment for Cr(VI) and Cd(II) from their 5 ppm mix solution was investigated at temperatures of 30, 40, and 50 °C. The solution had a constant pH of 6, with an mMOX dose of 10 mg in 10 mL solution, agitated for 120 min in a temperature-controlled shaker at 120 rpm for the study. The efficiency of the adsorbent was determined based on its adsorption capacity (q_e) and removal percentage (% R), which can be given by the following equations

$$q_e = \frac{(C_i - C_f)}{W} \times V \tag{1}$$

$$\% R = \frac{(C_i - C_f)}{C_i} \times 100 \tag{2}$$

where C_i, C_f, V, and W are the initial concentration of an analyte (mg/L), the final concentration of an analyte (mg/L), the volume of the solution (L), and weight of adsorbent (g), respectively.

■ **RESULTS AND DISCUSSION**

The preliminary adsorption experiment for selection of a suitable adsorbent was performed at pH 6, 30 °C, and a
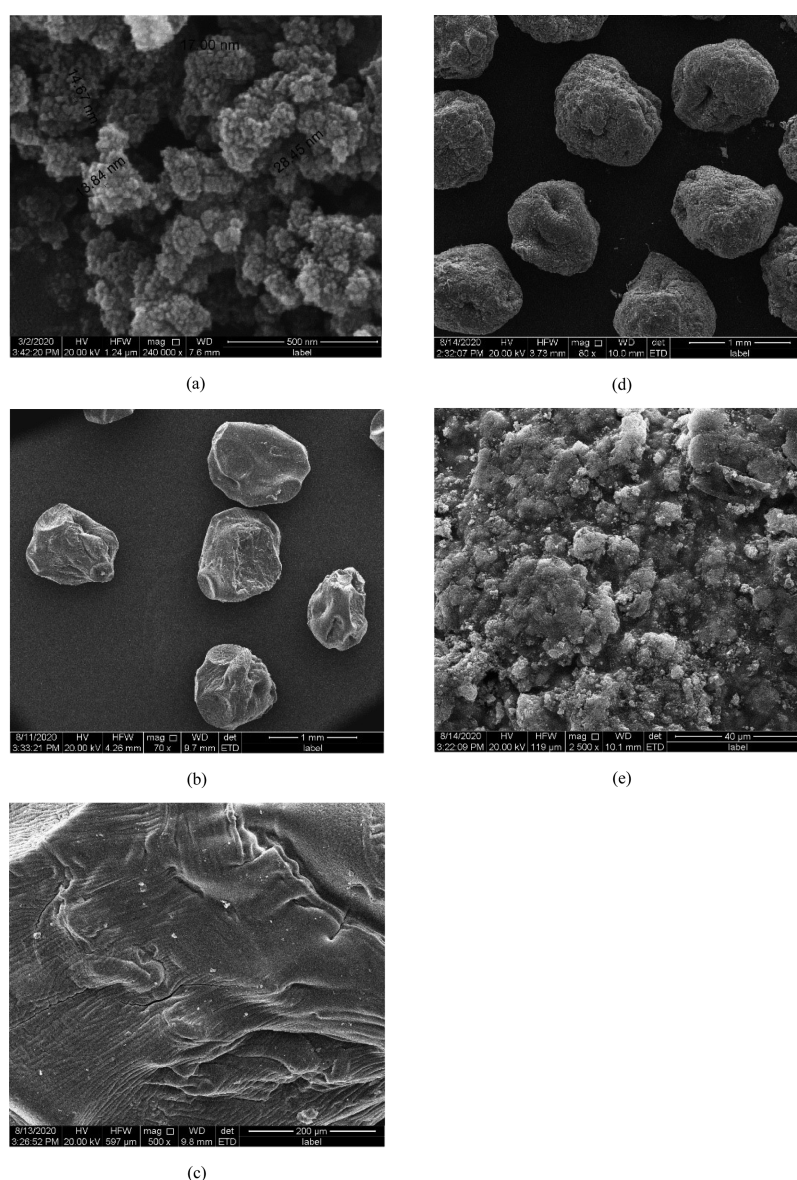
Figure 3. SEM images of the (a) mMO nanoparticles, (b,c) AX, and (d,e) mMOX.

contact time of 120 min. The % R of Cr(VI) and Cd(II) was found to be 67.3, 65.1; 57.3, 50.06; and 77.3, 81.8% for the AX, mMO nanoparticles, and mMOX, respectively. Thus, the mMOX was found to be the best adsorbent among them and was chosen for further adsorption studies. The removal percentages of Cr(VI) and Cd(II) at 30, 40, and 50 °C were found to be 77.31, 81.85; 66.34, 78.41; and 66.12, 70.07%, respectively. Therefore, adsorption and kinetic studies were carried out at 30 °C using 10 mg of the adsorbent mMOX in 10 mL solution of Cr(VI) and Cd(II).

Characterization. The surface area and pore volume of the adsorbent mMOX were analyzed using a surface area analyzer. Figure 1a,b shows its BET plot and nitrogen adsorption–desorption isotherms at a temperature of 77 K. The mean pore diameter, cumulative pore volume, and BET surface area of the mMOX were found to be 8.41 nm, 0.0491 cm^3/g, and 23.39 m^2/g, respectively. The hysteresis loop obtained from the graph suggests the type IV isotherm according to IUPAC classification, and the adsorbent is mesoporous.

Figure 2 represents the TGA plot of the mMOX, AX, and mMO nanoparticles. It was seen that there was a continuous loss in the weight of mMO nanoparticles from 50 to 250 °C. After 250 °C, the weight loss was minimal up to 750 °C, and after 790 °C, equilibrium was attained. The weight-loss trend of the mMOX was very similar to that of the bare AX. There was a rapid loss in the weight of both the gels between 190 and 300 °C. Both mMOX and AX suffered continuous weight loss between 290 and 790 °C, and after that, both the gels attained equilibrium. However, it was observed that the percentage weight loss of the mMOX was less compared to that of the AX. This was due to the high stability of the mMO nanoparticle that was coated on the bare AX. This showed that the mMOX is relatively stable to be used as an adsorbent.

The results obtained from SEM analysis of the magnetite nanoparticles, bare AX, and mMOX are presented in Figure 3. Figure 3a shows that the mMO nanoparticles are spherical, with an average size of 18 nm. From these images, it is visible that the nanoparticles get aggregated due to magnetic attraction between them. The bare AX (Figure 3b,c) had a
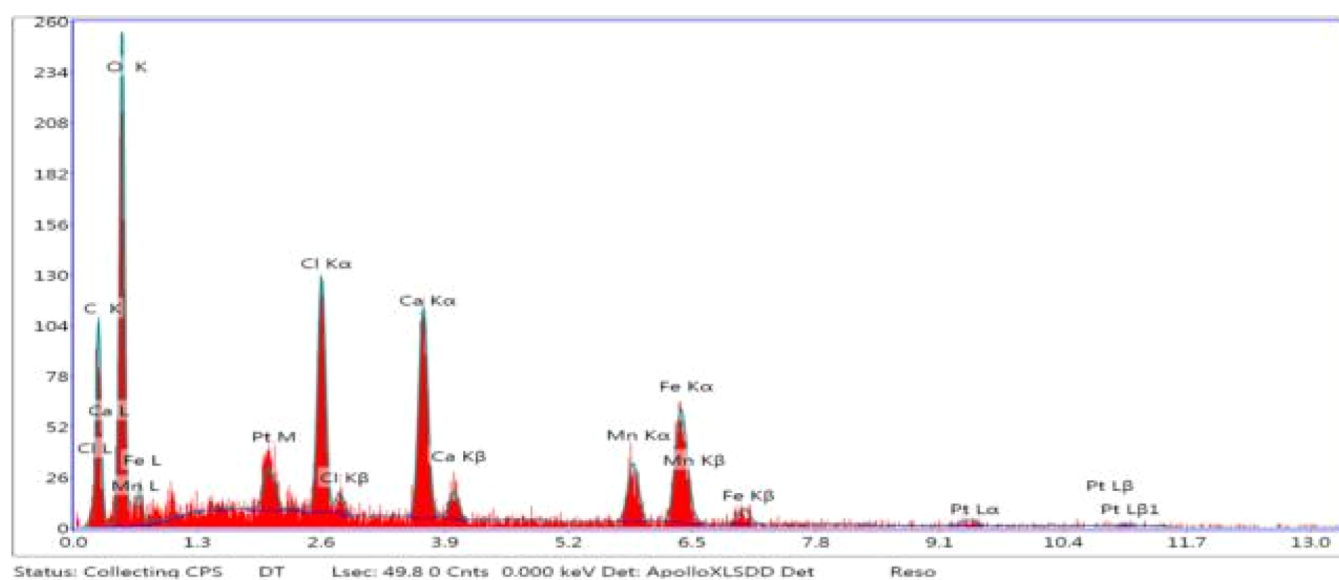
(a)
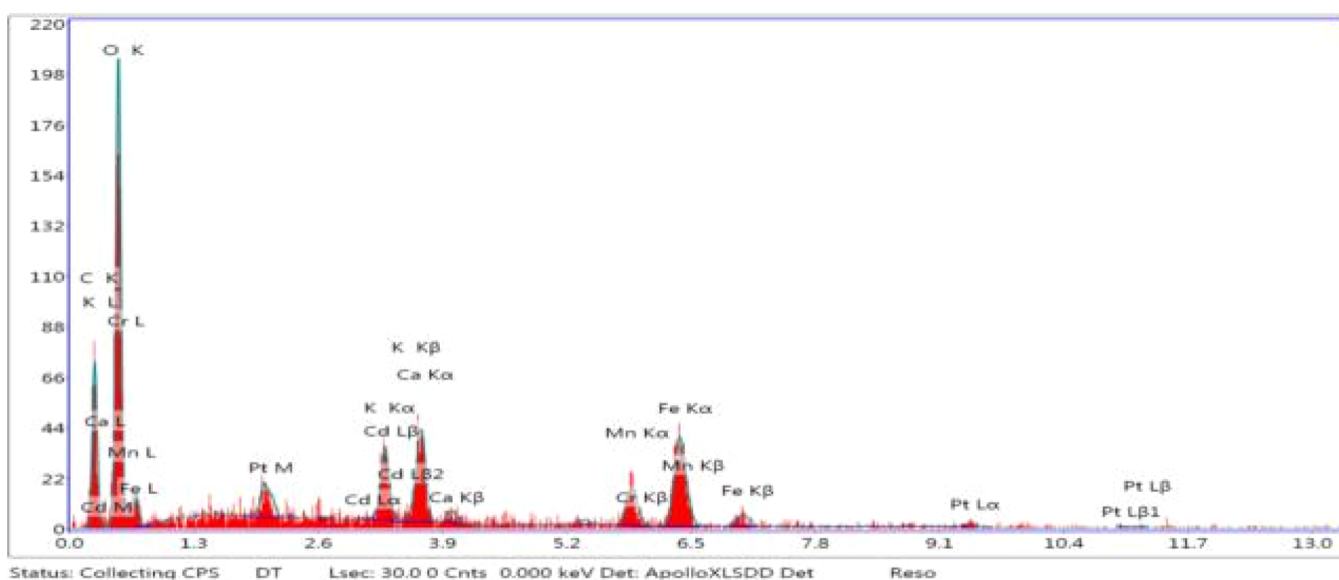
(b)

Figure 4. EDX of the (a) mMOX before adsorption and (b) mMOX after adsorption.

relatively smoother and plane surface than the mMOX (Figure 3d,e). The AX and mMOX have an average diameter of 1.046 and 1.167 mm, respectively. It is evident from the images that the mMOX had cracks, pores, and irregular and rough surfaces that could facilitate the diffusion of contaminants on them. The occurrence of cracks and pores in both AX and mMOX sample surfaces was probably due to the shrinkage of the gel on drying. Sigdel et al. also reported similar observations for hydrous iron oxide alginate beads.[23]

The elemental composition of the mMOX was obtained with the help of EDX (Figure 4 and Tables 1 and 2). EDX spectra of mMOX samples before and after the Cr and Cd adsorption are presented in Figure 4a,b, respectively. Detection of calcium (Ca) in the EDX spectrum of mMOx samples confirmed the sodium (Na) ion replacement by calcium ions

Table 1. Elemental Composition of the mMOX before Adsorption

| element	weight %	atomic %
C K	10.99	22.77
O K	33.54	52.01
ClK	9.08	6.35
CaK	11.61	7.18
MnK	6.96	3.14
FeK	15.99	7.1
PtL	11.83	1.5

via cross-linking. The presence of iron (Fe) and manganese (Mn) in the EDX spectrum (Figure 4a) confirmed the mMO nanoparticles' existence on the mMOX. Figure 4b shows the EDX spectra of the mMOX after adsorption of Cr and Cd. The

Table 2. Elemental Composition of the mMOX after Adsorption

element	weight %	atomic %
C K	12.69	22.85
O K	46.31	62.58
CdK	0.37	0.07
K K	3.98	2.2
CaK	5.87	3.17
CrK	0.45	0.19
MnK	5.27	2.07
FeK	14.86	5.75
PtL	10.2	1.13

peaks of Cr and Cd in the EDX spectra confirmed that Cr and Cd were adsorbed on the mMOX, which validated the application of this gel.

The point of zero charge (pzc) of mMO nanoparticles was obtained from a Zetasizer by measuring their zeta potential at different pH values ranging from 2 to 12. The determination of pzc helped in measuring the charge on the surface of the mMOX to establish that adsorption was occurring by electrostatic interactions.[30] Figure 5 shows the graph between zeta and pH. The pzc obtained from this was around 2.26.
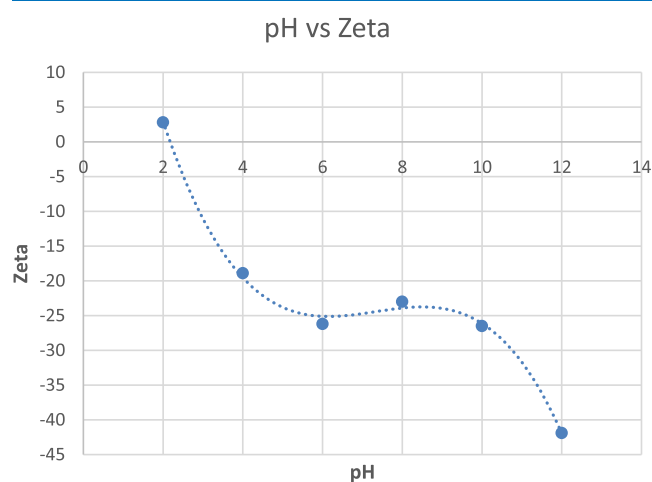
Figure 5. Effect of pH on zeta potential.

The FT-IR spectra of the mMO nanoparticles, AX, and mMOX were obtained at a wavelength ranging from 400 to 4000 cm^{-1} (Figure 6). Figure 6a shows the IR spectrum of mMO nanoparticles in which the peak at 3321 cm^{-1} is the characteristic stretching vibration peak of Fe−OH. The peak at 1646 cm^{-1} is due to stretching vibration from a combination of the Mn−O and −OH groups.[31] Figure 6b is the IR spectrum of the AX, in which a strong band at 3244 cm^{-1} was due to stretching of the −OH group of alginate. The appearance of strong bands at 1587 and 1416 cm^{-1} corresponds to asymmetric and symmetric stretching of the −COO (carboxyl) group of alginate, while the peak at 1025 cm^{-1} is due to stretching of the C−O−C bond.[32] Figure 6c indicates an IR spectrum of the mMOX in which a similar pattern of peaks (as of the AX) was observed, which showed that hydroxyl and carboxyl groups were retained after immobilization of mMO nanoparticles on the mMOX and adsorption of metal ions was occurring through these groups.

Parameters Affecting Adsorption of Cr and Cd. *Effect of Contact Time.* The adsorption of Cr and Cd was investigated at different interval of times. The dosage of the mMOX was fixed as 10 mg with a 5 ppm concentration of adsorbate solution. Figure 7 shows that after 30 min, more than 50% of Cr and 60% of Cd were removed. The adsorption capacity of the mMOX increased with time, and equilibrium was attained after 180 min, that is, 4.321 mg/g for Cr and 4.171 mg/g for Cd. The initial high rate of metal ion adsorption was due to abundance of active sites, which get decreased with the passing time.

Effect of pH. The adsorbate solution's pH plays a significant role in governing the adsorption of metal ions on the adsorbent. In our study, similar influence of pH on the adsorption of Cr and Cd was observed. 2−12 pH solutions of 5 ppm concentration of Cr and Cd were prepared using 0.1 N HCl and NaOH. An adsorbent dose of 10 mg of the mMOX in 10 mL was used for adsorption at constant time and temperature. Figure 8 shows the uptake of Cr and Cd with increasing pH. It can be seen from the figure that there was less adsorption of Cr and Cd at pH 2 and 4. This occurred because under acidic conditions, the active sites of the mMOX, which contain −OH and −COOH groups, become protonated, due to which the competition between H$^+$ ions and metal ions was increased to occupy the active sites. This caused electrostatic repulsion between the metal ions and adsorbent, resulting in lower uptake of Cr and Cd. This was also confirmed from the zeta values (Figure 5) that were positive at pH 2 (lower than pzc).

With the increase in pH of the solution, the surface of the mMOX became negatively charged (from Figure 5), which causes electrostatic attraction between metal ions and the adsorbent surface, and also, there was no competition from H$^+$ ions for active sites. The removal % of both Cr and Cd was maximum at pH 6, which again decreased with the increase in pH. This occurred due to the increase in the concentration of −OH ions, which resulted in the precipitation of poorly soluble metal hydroxides that did not get adsorbed on the adsorbent surface. Similar results were also reported by Idris et al. and de Castro Alves et al. for Pb(II) and Cd(II) ions.[33,34]

Effect of Adsorbent Dose. The % removal of Cr and Cd with an increasing adsorbent dose was studied at a contact time of 180 min, pH 6, and 5 ppm adsorbate concentration. The amount of adsorbent mMOX was varied between 10 and 100 mg. Figure 9 shows that % removal of both Cr and Cd was increased with an increased dosage of the mMOX. It was noted that 99% of Cr and 97% of Cd were removed by 100 mg of the mMOX. This increased uptake of metal ions by the adsorbent was basically due to an increase in the number of active surface sites.

Kinetic Study. In this study, kinetic data were fitted on the following models:[35]

(a) Pseudo-first-order model: The following equations can give a linear form of the pseudo-first-order model:

$$\ln(q_e - q_t) = \ln q_e - K_1 t \tag{3}$$

where q_t is the adsorption capacity at time t, q_e is the adsorption capacity at equilibrium, and K_1 is the first-order rate constant.

(b) Pseudo-second-order model: Its linear equation can be given as
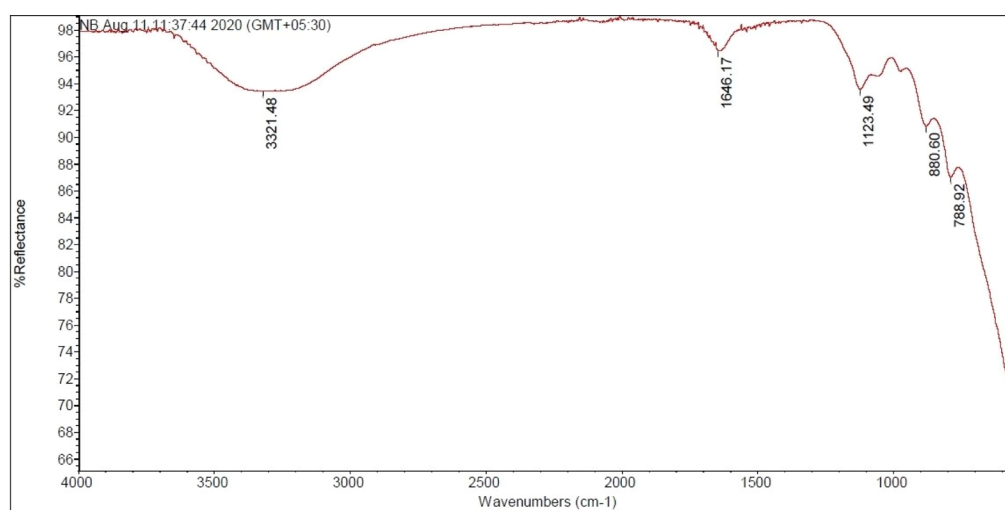
(a)

(b)

(c)

Figure 6. FT-IR spectra of the (a) mMO nanoparticles, (b) AX, and (c) mMOX.

Figure 7. Effect of contact time on % removal.

Figure 8. Effect of pH on % removal.

$$\frac{t}{q_t} = \frac{1}{K_2 q_e^2} + \frac{t}{q_e}$$

(4)

where k_2 is the second-order rate constant.

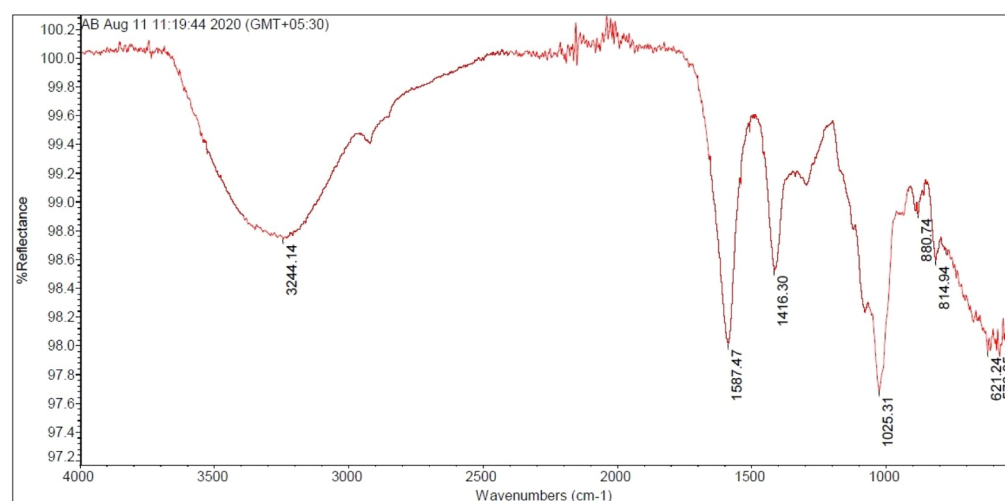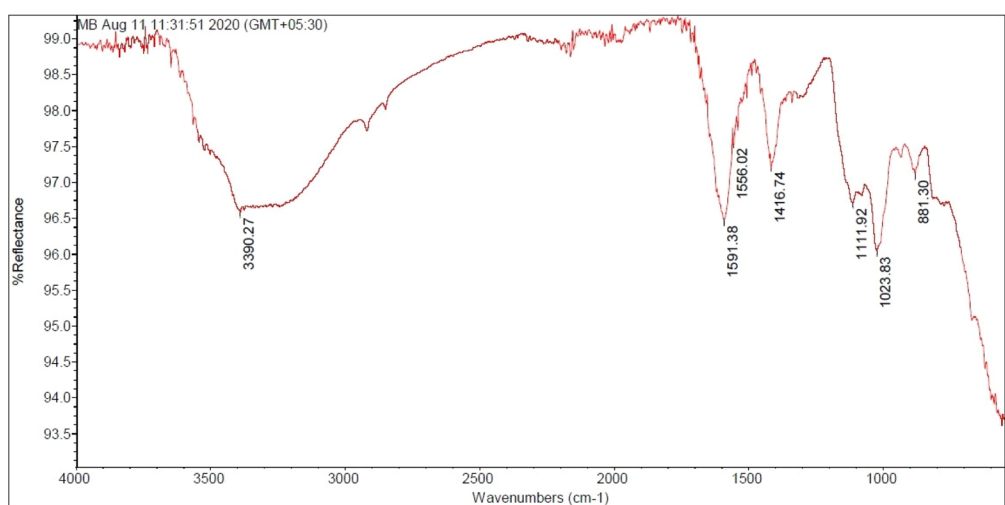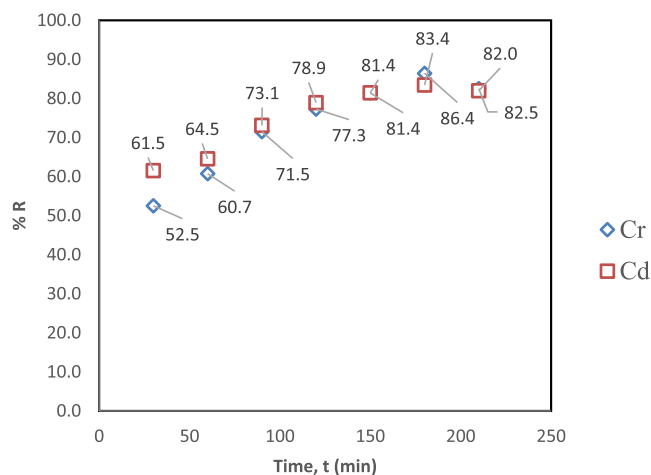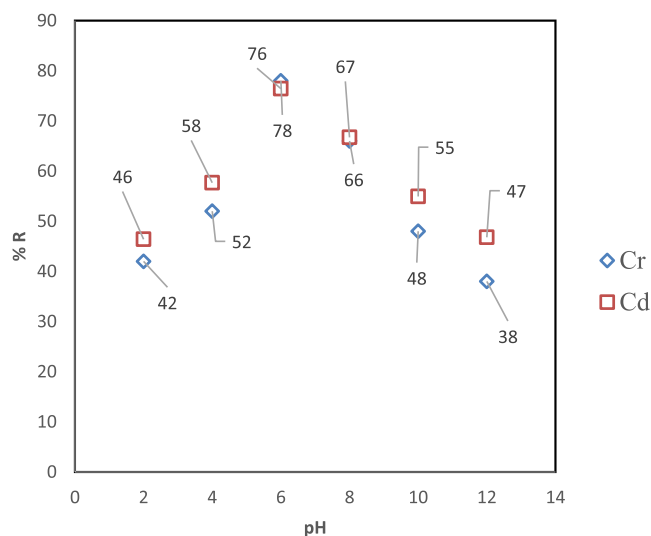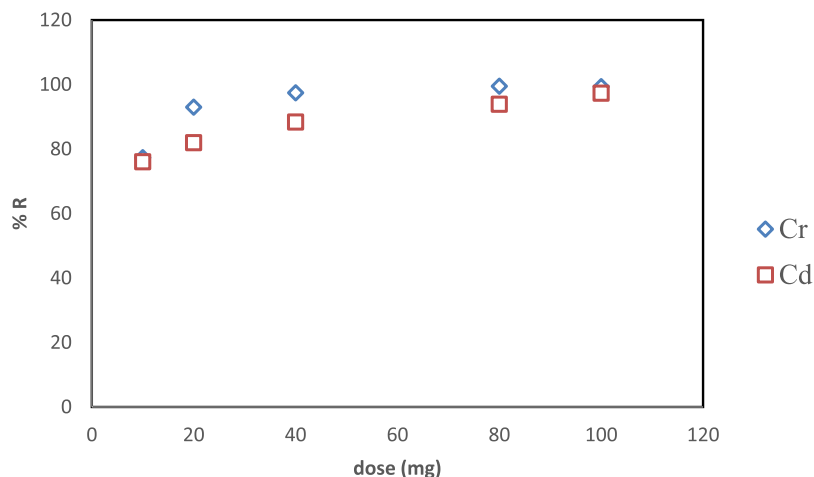(c) Intraparticle diffusion model: A linear form of Weber and Morris' intraparticle diffusion model can be given by

$$q_t = K_{id} t^{0.5} + C$$

(5)

where K_{id} is the intraparticle diffusion rate constant (mg/g min$^{0.5}$), $t^{0.5}$ is the half-life of adsorption, and C is the intercept that can be evaluated from the plot's slope between q_t and $t^{0.5}$

(d) Elovich kinetic model: Elovich equation for adsorption of the analyte can be given as

$$q_t = \frac{1}{\beta} \ln \alpha\beta + \frac{1}{\beta} \ln t$$

(6)

where α and β are the adsorption and desorption rate constants (in mg g^{-1} min^{-1}), respectively.

The abovementioned kinetic parameters were determined at 30 °C at different time intervals ranging from 30 to 180 min. Figure 10 shows the respective plots of pseudo-first-order, pseudo-second-order, intraparticle diffusion, and Elovich models with their parameters listed in Table 3. The observations showed that the data fitted best on the pseudo-second-order model having the R^2 value greater than 0.99. Furthermore, the R^2 value of intraparticle diffusion and Elovich models was found to be 0.966 and 0.992 (Cd and Cr, respectively) and 0.943 and 0.981 (Cd and Cr, respectively), which signifies the distribution of metal ions on the mMOX.

Adsorption Isotherms. In this study, adsorption isotherms were applied to the following models:[36]

(a) Langmuir adsorption isotherm: This isotherm assumes the surface of the adsorbent to be homogeneous and involves monolayer adsorption. Its equation can be given as

$$\frac{C_e}{q_e} = \frac{C_e}{q_m} + \frac{1}{K_a q_m}$$

(7)

where C_e is the equilibrium concentration, q_m is the maximum adsorption capacity, q_e is the adsorption capacity at equilibrium, and K_a is Langmuir's constant.

(b) Freundlich adsorption isotherm: This isotherm assumes the surface of the adsorbent to be heterogeneous. Its equation can be given as
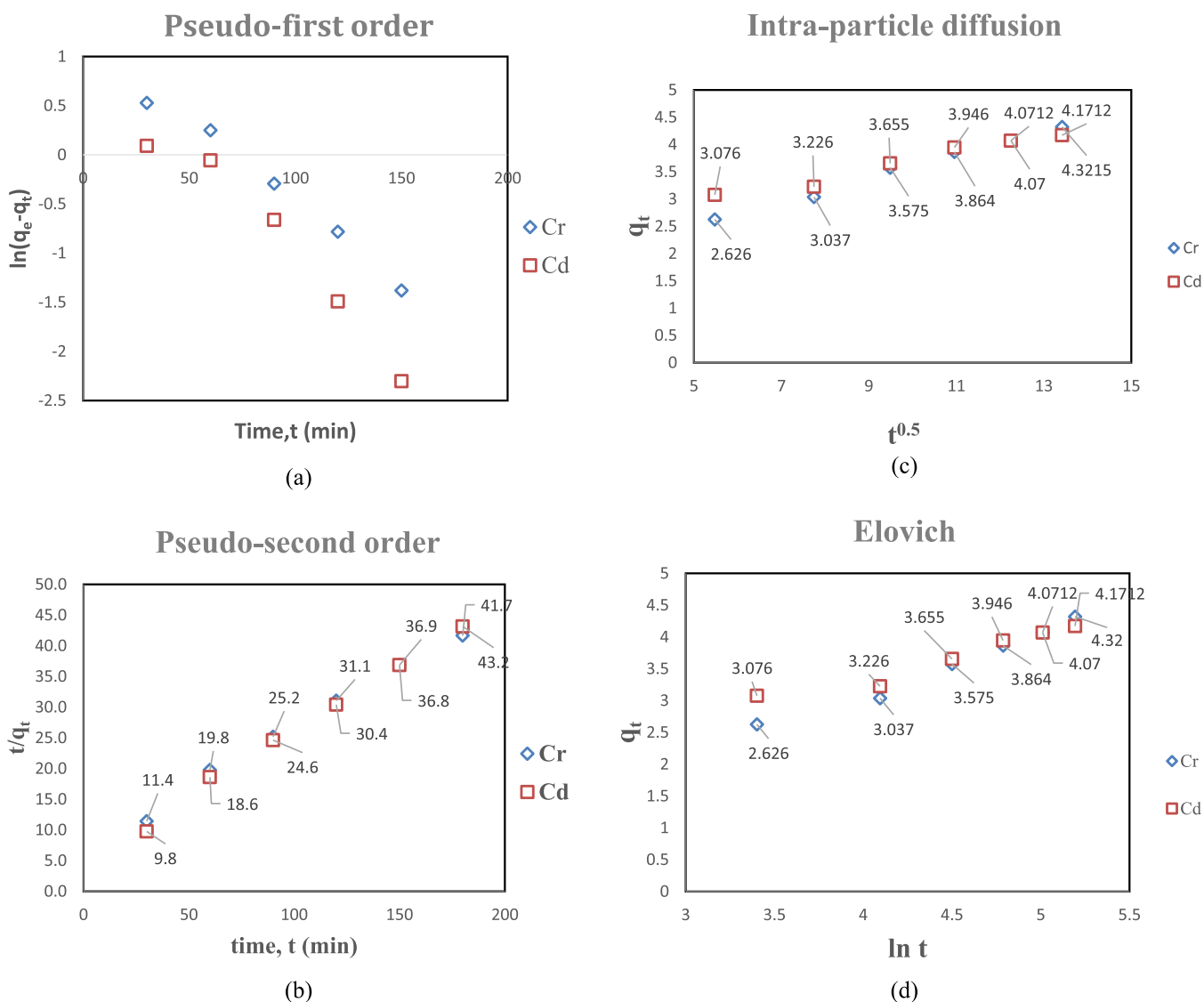

Figure 9. Effect of adsorbent dose on % removal.

Figure 10. Plots of (a) pseudo-first-order, (b) pseudo-second-order, (c) intraparticle diffusion, and (d) Elovich kinetic models.

Table 3. Parameters of Kinetic Isotherms

pseudo-first order	$\ln q_e$	q_{cal}	q_{exp}	K_1	R^2
Cd	0.98	2.67	4.17	0.02	0.952
Cr	1.12	3.06	4.32	0.016	0.987
pseudo-second order	$1/q_e$	q_{cal}	q_{exp}	K_2	R^2
Cd	0.21	4.61	4.17	0.01	0.996
Cr	0.198	5.04	4.32	0.006	0.993
intraparticle diffusion		K_{id}		R^2	
Cd		0.152		0.966	
Cr		0.2179		0.992	
Elovich	$1/\beta$	$1/\beta\ (\ln \alpha\beta)$	α	β	R^2
Cd	0.6671	0.6904	1.877	1.499	0.943
Cr	0.963	−0.7491	0.442	1.038	0.981

$$\log q_e = \log K_f + \frac{1}{n} \log C_e \tag{8}$$

where q_e is the adsorption capacity of the adsorbent, K_f is the Freundlich adsorption coefficient, C_e is the equilibrium concentration of the solution, and n is the exponential coefficient.

(c) Sips adsorption isotherm: It is applied for heterogeneous surfaces and combines Freundlich and Langmuir isotherms. It can be given as

$$\ln\left[\left(\frac{q_e}{q_m - q_e}\right)\right] = \frac{1}{n} \ln C_e + \ln K_s \tag{9}$$

where K_s is Sips' constant.

(d) Redlich−Peterson (R−P) adsorption isotherm: It can be applied for both homogeneous and heterogeneous surfaces. Its equation can be given as

$$\frac{C_e}{q_e} = \frac{a}{K_P} C^b + 1/K_P \tag{10}$$

where a, b, and K_P are Redlich−Peterson constants.

(e) Temkin adsorption isotherm: It states that the heat of adsorption decreases with layer coverage. It can be expressed as

$$q_e = \frac{RT}{b} \ln A + \frac{RT}{b} \ln C_e \tag{11}$$

where R is the gas constant, T is temperature, and A and b are Temkin constants.

(f) Dubinin−Radushkevich (D−R) adsorption isotherm: It is applicable for the porous heterogeneous surface and can be given as[37]

$$\ln q_e = \ln q_m - K\varepsilon^2 \tag{12}$$

$$\varepsilon = RT \ln\left(1 + \frac{1}{C}\right) \tag{13}$$

$$E = 1/\sqrt{2K} \tag{14}$$

where K is the constant, and ε is the Polanyi potential, R is the gas constant, C is the concentration of a solution, and E is the bonding energy of the adsorbate and adsorbent.

The adsorption data were fitted on the abovementioned isotherm models with their respective parameters listed in Table 4. Figure 11 shows the individual plots of Langmuir,

Table 4. Parameters of Adsorption Isotherms

Langmuir	$1/q_m$	q_m	$1/K_a q_m$	K_a	R^2
Cd	0.13	7.79	0.22	0.57	0.95
Cr	0.14	7.24	0.32	0.43	0.86
Freundlich	$1/n$	n	$\log K_f$	K_f	R^2
Cd	0.58	1.70	0.40	2.52	0.99
Cr	0.47	2.134	0.37	2.35	0.94
D−R	K	$\ln q_m$	q_m	E	R^2
Cd	−0.072	1.51	4.54	2.63	0.89
Cr	−0.187	1.53	4.59	1.63	0.79
Temkin	b	$RT/b \ln A$	$\ln A$	A	R^2
Cd	1.68	3.15	2.11	8.26	0.94
Cr	1.31	2.46	1.28	3.62	0.92
Sips	$1/n$	n	$\ln K_S$	K_S	R^2
Cd	0.94	1.05	−0.51	0.59	0.97
Cr	1.82	0.54	−0.44	0.64	0.64
R−P	$1/K_P$	a/K_P	a	B	R^2
Cd	0.128	0.078	0.60	0.90	0.96
Cr	0.168	0.101	0.60	0.90	0.8146

Freundlich, Temkin, Sips, R−P, and D−R adsorption isotherms. Isotherm modeling was carried out with the initial concentration ranging from 1 to 10 ppm and a contact time of 180 min. Figure 11a,b shows that the adsorption data fitted both Langmuir and Freundlich isotherms. However, it worked best on the Freundlich model due to its high R^2 value. The maximum adsorption capacities (q_m) for Cr and Cd from the Langmuir model were found to be 7.24 and 7.79 mg/g, respectively. The separation factor (R_L) of the Langmuir model can be given as[38]

$$R_L = \frac{1}{1 + K_a C_i} \tag{15}$$

where K_a and C_i are the Langmuir constant and initial concentration, respectively.

For favorable adsorption, the value of R_L should lie between 0 and 1,[39] which, in this study, was found to be 0.95, 0.86, 0.79, 0.73, 0.68, and 0.66 for Cr and 0.91, 0.71, 0.67, 0.59, 0.53, and 0.51 for Cd and indicated a favorable adsorption. From the Freundlich model, the value of n was found to be 2.134 (for Cr) and 1.70 (for Cd), which lied between 1 and 10 and

suggested favorable adsorption.[40] From Table 4, the Sips model's high R^2 value for both Cr and Cd suggested that the experimental data fitted both Freundlich and Langmuir models. The value of E in the D−R model indicates the physisorption phenomenon. This also validated that this could be due to roughness or cracks in the synthesized xerogel that facilitated the adsorption of Cr(VI) and Cd(II). If the value of E is less than 8 kJ/g, then the adsorption is physical, while if it is in between 8 and 16 kJ/g, then it is chemisorption.[41] In this study, the values of Cd and Cr were 2.63 and 1.63 kJ/g, respectively, which indicated the physisorption mechanism. The R^2 values were also found to be high for Temkin, followed by R−P and Sips models.

Thermodynamics of Adsorption. The thermodynamic study was carried out in this work with the help of Gibbs and Van't Hoff equations that can be given as[42]

$$\Delta G = -RT \ln K_0 \tag{16}$$

$$K_0 = C_a/C_S \tag{17}$$

$$\Delta G = \Delta H - T\Delta S \tag{18}$$

where ΔG is Gibbs free energy, ΔH is enthalpy change, ΔS is entropy change, T is temperature change, R is the gas constant, K_0 is the equilibrium constant, and C_a and C_S are the concentrations of the adsorbate on the adsorbent and solution, respectively. The thermodynamic parameters, namely, ΔH, ΔS, and ΔG, are given in Table 5. The negative values of ΔH and ΔS indicated an exothermic process, while the negative values of ΔG showed that the adsorption phenomenon is spontaneous.[43]

Regeneration and Reuse of the Adsorbent. The adsorbent was regenerated using 0.1 N HCl since the adsorption capacity of the mMOX was less at a low pH range. The adsorbent (mMOX) was added in 0.1 N HCl, and the mixture was shaken at 120 rpm for 2 h. The adsorbent was then dried and used again for Cr(VI) and Cd(II) adsorption from 5 ppm solution, which was the first cycle of adsorption. Similarly, the performance of mMOX was observed for six regeneration cycles in adsorption of Cr(VI) and Cd(II). A number of regeneration cycles with their % R are listed in Table 6 which shows that after six cycles, more than 55% removal of Cr and more than 60% removal of Cd were achieved. This showed that mMOX had good reusability, making it an economical adsorbent. The decrease in % R of mMOX could be due to incomplete desorption of Cr and Cd ions that resulted in a reduced number of vacant sites.

Leaching Study. The leaching study was conducted to observe whether metal ions (Fe, Na, Ca, K, and Mn) from the adsorbent are leaching into the aqueous solution or not. If metal ions leach into the solution, they would contaminate the water, and inevitably, the adsorbent would become useless. For this, 20 mg of the mMOX was added to 10 mL of Milli-Q water, and the mixture was shaken at 120 rpm for 5 h. The concentration of metal ion leaching from the mMOX is listed in Table 7. The observation showed that calcium, sodium, and manganese ions are leaching into the water, but they are under their maximum permissible limits in drinking water, while there was no leaching of Fe and K, which suggests that the mMOX can be used safely for Cr and Cd removal from water. It can be seen that a high amount of iron, manganese, and potassium is leaching from mMO nanoparticles, while sodium is leaching from the AX, which is one of the main reasons that they are not used as the adsorbing material in this study.
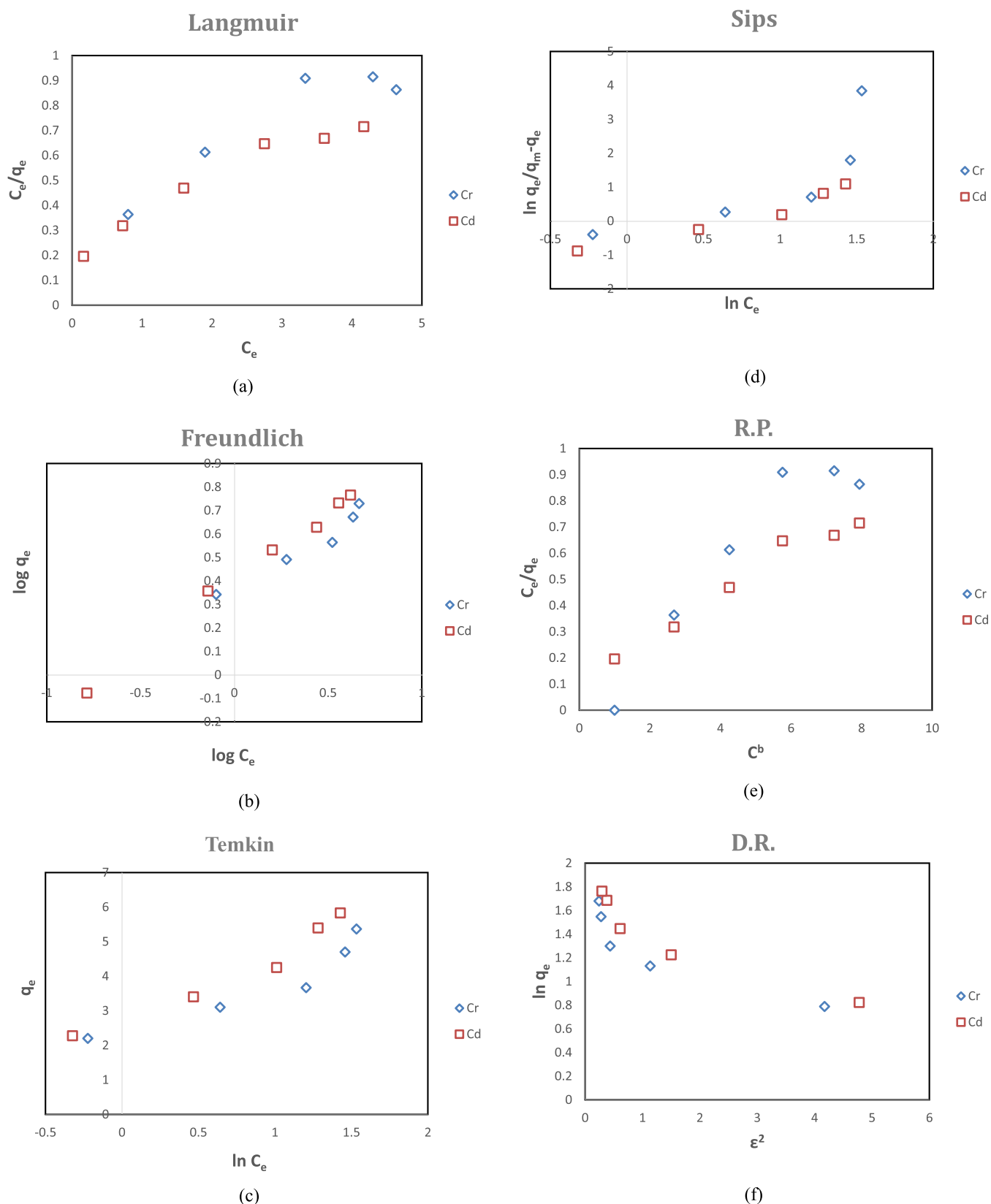
Figure 11. Plots of (a) Langmuir, (b) Freundlich, (c) Temkin, (d) Sips, (e) R–P, and (f) D–R.

Application of the mMOX in Real Water Samples and Its Nonselectivity toward Interfering Metals. Water samples were collected one day before the experiment from the Gomti River, Lucknow, India. The analysis of Cr, Cd, Na, K, and Mg before and after adsorption by the mMOX was carried out in these samples, and the results are listed in Table S1. Low concentrations of these metals were found. Therefore, the samples were spiked with known metal ion concentrations and

Table 5. Parameters of Thermodynamics Study

temperature	ΔG	ΔH	ΔS
30	−3.09	−22.90	−0.07
40	−1.76		
50	−1.78		

Table 6. % Removal of Cr and Cd for Regeneration Cycles

no. of cycles	% R of Cr	% R of Cd
1	77.3	76.23
2	70	71.5
3	70.7	71.04
4	62.67	67.56
5	56	64.23
6	57	61.45

Table 7. Concentration of Ions Leaching from Adsorbents

s. no.	sample name	calcium (concn mg/L)	sodium (concn mg/L)	iron (concn mg/L)	manganese (concn mg/L)	potassium (concn mg/L)
1	AX	41.93	549.33	0	0	0
2	mMOX	15.75	63.67	0	27.5	0
3	mMO	0	14.5	987.5	2100	298.83

then analyzed after adsorption by the mMOX. Table 8 shows that 69.56−82.82% of Cr and 63.4−77.2% of Cd were removed by 10 mg of the mMOX in 10 mL solution with a contact time of 120 min. It was to be noted that the % removal of Na, K, and Mg was less than 25% (Table 9) from most of the samples, and among them, Na was adsorbed less than 10% in all samples. The samples with their metal concentration, % removal, and adsorption capacities of the mMOX are given in Tables 7 and 9.

It can be seen from Table 9 that the mMOX is not effective in adsorbing sodium, potassium, and magnesium ions with % R ranging from 3.5 to 16.2% for Na, 0−40.5% for K, and 6.9−33.6% for Mg. This shows that the prepared xerogel mMOX is highly selective in the removal of Cr(VI) and Cd(II) ions. Table 10 shows the application of different adsorbents in removal of Cr and Cd.

CONCLUSIONS

In this work, mMO nanoparticles were synthesized by the co-precipitation method and characterized by SEM−EDX, FTIR, Zetasizer, and BET. These nanoparticles were successfully immobilized on alginate, producing the mMOX. This xerogel was also characterized by SEM−EDX, FTIR, Zetasizer, and BET. The performance of the mMOX for the adsorption of Cr(VI) and Cd(II) was investigated at different temperatures, pH values, time of contact, initial concentration of the adsorbate, and the dose of the adsorbent. The kinetic and isotherm modeling was carried out by a nonlinear method, which indicated the physisorption mechanism. The kinetic data fitted well on pseudo-second order, while adsorption data fitted on the Freundlich isotherm. The thermodynamic study revealed the adsorption to be spontaneous and exothermic. The regeneration study indicated that the mMOX could be reused up to six cycles with more than 50% removal of Cr and Cd. The adsorbent showed useful application on real water samples by more than 75% uptake of Cr and Cd with low adsorption of Na, K, and Mg.

A future study could be conducted by modifying the adsorbent to increase its performance in terms of adsorption capacity and % removal by consuming less time than this study. Furthermore, heavy metals could also be explored for their adsorption on this xerogel.

MATERIALS AND METHODS

Analytical grade anhydrous ferrous sulfate heptahydrate ($FeSO_4 \cdot 7H_2O$), potassium permanganate ($KMnO_4$), ethanol (C_2H_5OH), calcium chloride ($CaCl_2$), cadmium chloride ($CdCl_2$), potassium dichromate ($K_2Cr_2O_7$), and sodium alginate were procured from Sigma-Aldrich, USA. Analytical grade sodium hydroxide (NaOH), concentrated nitric acid, and hydrochloric acid were obtained from Merck, Darmstadt, Germany. All experiments were conducted using Milli-Q water obtained from CSIR-IITR, India. Certified reference standards of heavy metals were purchased from Merck, Darmstadt, Germany. The stock solution of heavy metal standard was diluted to prepare the calibration standard for quantification of metals. Study was conducted in triplicate along with the sample and reagent blank.

Table 8. % Removal of Cr and Cd from Real Water Samples

sample no.	concn of Cr (ppm)	concn of Cr after adsorption (ppm)	concn of Cd (ppm)	concn of Cd after adsorption (ppm)	% removal of Cr	% removal of Cd
1	4.6	1.3	4.3	1.5	71.7	67.0
2	4.6	1.3	4.4	1.5	71.7	66.1
3	4.6	1.3	4.5	1.5	71.7	66.1
4	4.6	1.4	4.5	1.6	69.6	65.0
5	4.6	1.4	4.4	1.6	69.6	64.5
6	4.7	1.1	4.5	1.4	76.6	69.8
7	4.5	1.3	4.4	1.6	71.1	65.4
8	4.6	1.3	4.5	1.5	71.7	66.2
9	4.7	1.3	4.5	1.5	72.3	66.4
10	4.6	1.3	4.4	1.5	71.7	65.2
11	4.6	1.1	4.5	1.3	76.1	70.9
12	4.6	0.8	4.4	1.1	82.8	76.8
13	4.7	0.9	4.4	1.2	80.6	73.5
14	4.7	0.8	4.5	1.1	82.8	77.2
15	4.7	1.4	4.6	1.7	70.2	63.4

Table 9. % Removal of Na, K, and Mg from Real Water Samples

sample no.	sodium			potassium			magnesium		
	initial concn (ppm)	final concn (ppm)	% removal	initial concn (ppm)	final concn (ppm)	% removal	initial concn (ppm)	final concn (ppm)	% removal
1	3.5	3.3	4.9	4.5	4.5	0.0	4.8	3.3	30.0
2	3.2	3.4	−6.9	4.7	4.2	11.1	4.8	3.2	33.6
3	3.8	3.2	16.2	5.0	4.6	7.7	4.8	3.5	27.5
4	3.5	3.4	3.5	4.6	4.6	0.0	5.0	4.4	11.4
5	3.3	3.2	3.0	4.8	2.9	38.8	4.8	4.3	9.9
6	3.5	3.3	6.4	4.7	3.2	32.1	4.9	3.3	31.7
7	3.5	3.4	5.1	4.4	3.1	31.0	4.8	3.9	20.1
8	3.5	3.2	8.2	4.8	4.4	9.1	4.8	3.7	23.8
9	3.5	3.3	5.2	4.4	4.2	6.0	4.9	4.1	16.3
10	3.3	3.2	4.5	4.7	3.1	34.1	4.7	4.4	7.6
11	3.5	3.4	3.7	5.2	3.1	40.5	4.8	3.3	32.1
12	3.7	3.4	6.0	5.0	3.2	37.0	4.8	3.6	24.3
13	3.4	3.2	5.5	4.7	4.1	11.3	4.9	3.7	25.0
14	3.6	3.3	9.3	5.9	4.0	32.1	4.9	4.4	10.3
15	3.2	3.3	−1.2	4.9	4.2	13.6	4.9	4.5	6.9

Table 10. Comparison of Cr(VI) and Cd(II) Adsorption on Various Adsorbents

s. no.	adsorbent	adsorbate	adsorption capacity	references
1	alginate-Ayous wood sawdust (*Triplochiton scleroxylon*)	Cd(II)	6.21	44
2	*Ambrosia trifida* L. var. trifida biochar-alginate beads (ATLB-AB)	Cd(II)	9.73	45
3	amino-functionalized magnetite/kaolin clay	Cd(II)	13.1	46
4	polyvinyl alcohol-S.A. beads	Cd(II)	0.52	47
5	montmorillonite-supported magnetite nanoparticles	Cr(VI)	15.3	48
6	magnetite−magnetite nanoparticles	Cr(VI)	2.4	49
7	Fe$_3$O$_4$@Alg-Ce magnetic beads	Cr(VI)	9.166	50
8	bio polymeric beads	Cr(VI)	0.833	51
9	magnetite−manganese oxide xerogel (mMOX)	Cd(II)	7.79	this work
10	magnetite−manganese oxide xerogel (mMOX)	Cr(VI)	7.24	this work

■ ASSOCIATED CONTENT

Ⓢ Supporting Information

The Supporting Information is available free of charge at https://pubs.acs.org/doi/10.1021/acsomega.0c05787.

Analysis of metals in real samples (PDF)

■ AUTHOR INFORMATION

Corresponding Authors

Nasreen G. Ansari − *Analytical Chemistry Laboratory, Regulatory Toxicology Group, CSIR-Indian Institute of Toxicology Research, (CSIR-IITR), Lucknow 226001, Uttar Pradesh, India; Academy of Scientific and Innovative Research (AcSIR), Ghaziabad 201002, India;* ⓞ orcid.org/0000-0003-3495-2360; Email: nasreen@iitr.res.in

Devendra K. Patel − *Analytical Chemistry Laboratory, Regulatory Toxicology Group, CSIR-Indian Institute of Toxicology Research, (CSIR-IITR), Lucknow 226001, Uttar Pradesh, India; Academy of Scientific and Innovative Research (AcSIR), Ghaziabad 201002, India;* Email: dkpatel@iitr.res.in

Authors

Aditya Kumar − *Analytical Chemistry Laboratory, Regulatory Toxicology Group, CSIR-Indian Institute of Toxicology Research, (CSIR-IITR), Lucknow 226001, Uttar Pradesh, India; Academy of Scientific and Innovative Research (AcSIR), Ghaziabad 201002, India*

Satgur Prasad − *Analytical Chemistry Laboratory, Regulatory Toxicology Group, CSIR-Indian Institute of Toxicology Research, (CSIR-IITR), Lucknow 226001, Uttar Pradesh, India*

Prem N. Saxena − *Electron Microscopy, CSIR-Indian Institute of Toxicology Research, (CSIR-IITR), Lucknow 226001, Uttar Pradesh, India*

Complete contact information is available at:
https://pubs.acs.org/10.1021/acsomega.0c05787

Author Contributions

N.G.A. and D.K.P. contributed equally. A.K.—methodology, experimentation, data curation, and writing. S.P. and P.N.S.—formal analysis and data curation. N.G.A. and D.K.P.—conceptualization, supervision, resources, and writing, review and editing.

Notes

The authors declare no competing financial interest.

■ ACKNOWLEDGMENTS

BET surface area analyzer, TGA, Zetasizer, SEM−EDX, and ATR-FTIR.

ABBREVIATIONS

AX, alginate xerogel; mMO, magnetite−manganese oxide; mMOX, magnetite−manganese oxide xerogel; pzc, point of zero charge; ppm, parts per million

REFERENCES

(1) Kanamarlapudi, S. L. R. K.; Chintalpudi, V. K.; Muddada, S. Application of biosorption for removal of heavy metals from wastewater. *Biosorption* **2018**, *18*, 69−116.

(2) Krause-Nehring, J.; Brey, T.; Thorrold, S. R. Centennial records of lead contamination in northern Atlantic bivalves (Arctica islandica). *Mar. Pollut. Bull.* **2012**, *64*, 233−240.

(3) Adebayo, I. A. Determination of heavy metals in water, fish and sediment from Ureje water reservoir. *Fish & Ocean Opj* **2017**, *7*, 555628.

(4) Zhang, Y.; Griffin, A.; Rahman, M.; Camper, A.; Baribeau, H.; Edwards, M. Lead contamination of potable water due to nitrification. *Environ. Sci. Technol.* **2009**, *43*, 1890−1895.

(5) Deb, A. K. S.; Dwivedi, V.; Dasgupta, K.; Ali, S. M.; Shenoy, K. Novel amidoamine functionalized multi-walled carbon nanotubes for removal of mercury (II) ions from wastewater: combined experimental and density functional theoretical approach. *Chem. Eng. J.* **2017**, *313*, 899−911.

(6) Shekhawat, K.; Chatterjee, S.; Joshi, B. Chromium toxicity and its health hazards. *Int. J. Adv. Res.* **2015**, *3*, 167−172.

(7) Wang, X. S.; Chen, L. F.; Li, F. Y.; Chen, K. L.; Wan, W. Y.; Tang, Y. J. Removal of Cr (VI) with wheat-residue derived black carbon: reaction mechanism and adsorption performance. *J. Hazard. Mater.* **2010**, *175*, 816−822.

(8) Rahimzadeh, M. R.; Rahimzadeh, M. R.; Kazemi, S.; Moghadamnia, A.-a. Cadmium toxicity and treatment: An update. *Caspian J. Intern. Med.* **2017**, *8*, 135−145.

(9) Patrick, L. Toxic metals and antioxidants: Part II. The role of antioxidants in arsenic and cadmium toxicity. *Alternative Med. Rev.* **2003**, *8*, 106−128.

(10) Thabede, P. M.; Shooto, N. D.; Xaba, T.; Naidoo, E. B. Adsorption studies of toxic cadmium (II) and chromium (VI) ions from aqueous solution by activated black cumin (Nigella sativa) seeds. *J. Environ. Chem. Eng.* **2020**, *8*, 104045.

(11) Akpor, O. B.; Ohiobor, G. O.; Olaolu, D. Heavy metal pollutants in wastewater effluents: sources, effects and remediation. *Adv. Biosci. Bioeng.* **2014**, *2*, 37−43.

(12) Hawley, E. L.; Deeb, R. A.; Kavanaugh, M. C.; Jacobs, J. A. Treatment technologies for chromium (VI). *Chromium (VI) Handb.* **2004**, *275*, 309−319.

(13) Friedrich, K. A.; Henglein, F.; Stimming, U.; Unkauf, W. Investigation of Pt particles on gold substrates by IR spectroscopy particle structure and catalytic activity. *Colloids Surf., A* **1998**, *134*, 193−206.

(14) Di Natale, F.; Gargiulo, V.; Alfè, M. Adsorption of heavy metals on silica-supported hydrophilic carbonaceous nanoparticles (SHNPs). *J. Hazard. Mater.* **2020**, *393*, 122374.

(15) Heidari, A.; Younesi, H.; Mehraban, Z.; Heikkinen, H. Selective adsorption of Pb(II), Cd(II), and Ni(II) ions from aqueous solution using chitosan-MAA nanoparticles. *Int. J. Biol. Macromol.* **2013**, *61*, 251−263.

(16) Maponya, T. C.; Ramohlola, K. E.; Kera, N. H.; Modibane, K. D.; Maity, A.; Katata-Seru, L. M.; Hato, M. J. Influence of Magnetic Nanoparticles on Modified Polypyrrole/m-Phenylediamine for Adsorption of Cr(VI) from Aqueous Solution. *Polymers* **2020**, *12*, 679.

(17) Vilardi, G.; Mpouras, T.; Dermatas, D.; Verdone, N.; Polydera, A.; Di Palma, L. Nanomaterials application for heavy metals recovery from polluted water: The combination of nano zero-valent iron and carbon nanotubes. Competitive adsorption non-linear modeling. *Chemosphere* **2018**, *201*, 716−729.

(18) Liu, L.; Luo, X.-B.; Ding, L.; Luo, S.-L. Application of nanotechnology in the removal of heavy metal from water. *Nanomater. Removal Pollut. Resour. Reutil.* **2019**, 83−147.

(19) Badruddoza, A. Z. M.; Shawon, Z. B. Z.; Tay, W. J. D.; Hidajat, K.; Uddin, M. S. Fe3O4/cyclodextrin polymer nanocomposites for selective heavy metals removal from industrial wastewater. *Carbohydr. Polym.* **2013**, *91*, 322−332.

(20) Zhao, J.; Liu, J.; Li, N.; Wang, W.; Nan, J.; Zhao, Z.; Cui, F. Highly efficient removal of bivalent heavy metals from aqueous systems by magnetic porous Fe3O4-MnO2: Adsorption behavior and process study. *Chem. Eng. J.* **2016**, *304*, 737−746.

(21) Zhao, Z.; Liu, J.; Cui, F.; Feng, H.; Zhang, L. One pot synthesis of tunable Fe 3 O 4−MnO 2 core−shell nanoplates and their applications for water purification. *J. Mater. Chem.* **2012**, *22*, 9052−9057.

(22) Luo, X.; Wang, C.; Luo, S.; Dong, R.; Tu, X.; Zeng, G. Adsorption of As (III) and As (V) from water using magnetite Fe3O4-reduced graphite oxide−MnO2 nanocomposites. *Chem. Eng. J.* **2012**, *187*, 45−52.

(23) Sigdel, A.; Park, J.; Kwak, H.; Park, P.-K. Arsenic removal from aqueous solutions by adsorption onto hydrous iron oxide-impregnated alginate beads. *J. Ind. Eng. Chem.* **2016**, *35*, 277−286.

(24) Stoica-Guzun, A.; Stroescu, M.; Jinga, S. I.; Mihalache, N.; Botez, A.; Matei, C.; Berger, D.; Damian, C. M.; Ionita, V. Box-Behnken experimental design for chromium(VI) ions removal by bacterial cellulose-magnetite composites. *Int. J. Biol. Macromol.* **2016**, *91*, 1062−1072.

(25) Thakur, S.; Sharma, B.; Verma, A.; Chaudhary, J.; Tamulevicius, S.; Thakur, V. K. Recent progress in sodium alginate based sustainable hydrogels for environmental applications. *J. Cleaner Prod.* **2018**, *198*, 143−159.

(26) Park, H. G.; Kim, T. W.; Chae, M. Y.; Yoo, I.-K. Activated carbon-containing alginate adsorbent for the simultaneous removal of heavy metals and toxic organics. *Process Biochem.* **2007**, *42*, 1371−1377.

(27) Lin, S.; Huang, R.; Cheng, Y.; Liu, J.; Lau, B. L. T.; Wiesner, M. R. Silver nanoparticle-alginate composite beads for point-of-use drinking water disinfection. *Water Res.* **2013**, *47*, 3959−3965.

(28) Job, N.; Théry, A.; Pirard, R.; Marien, J.; Kocon, L.; Rouzaud, J.-N.; Béguin, F.; Pirard, J.-P. Carbon aerogels, cryogels and xerogels: Influence of the drying method on the textural properties of porous carbon materials. *Carbon* **2005**, *43*, 2481−2494.

(29) Zhu, J.; Baig, S. A.; Sheng, T.; Lou, Z.; Wang, Z.; Xu, X. Fe3O4 and MnO2 assembled on honeycomb briquette cinders (HBC) for arsenic removal from aqueous solutions. *J. Hazard. Mater.* **2015**, *286*, 220−228.

(30) Kumar, S.; Nair, R. R.; Pillai, P. B.; Gupta, S. N.; Iyengar, M. A. R.; Sood, A. K. Graphene oxide−MnFe2O4 magnetic nanohybrids for efficient removal of lead and arsenic from water. *ACS Appl. Mater. Interfaces* **2014**, *6*, 17426−17436.

(31) Li, Q.; Yang, F.; Zhang, J.; Zhou, C. Magnetic Fe 3 O 4/MnO 2 core−shell nano-composite for removal of heavy metals from wastewater. *SN Appl. Sci.* **2020**, *2*, 1375.

(32) Sadiq, A.; Choubey, A.; Bajpai, A. K. Biosorption of chromium ions by calcium alginate nanoparticles. *J. Chil. Chem. Soc.* **2018**, *63*, 4077−4081.

(33) de Castro Alves, L.; Yáñez-Vilar, S.; Piñeiro-Redondo, Y.; Rivas, J. Novel magnetic nanostructured beads for cadmium (II) removal. *Nanomaterials* **2019**, *9*, 356.

(34) Idris, A.; Ismail, N. S. M.; Hassan, N.; Misran, E.; Ngomsik, A.-F. Synthesis of magnetic alginate beads based on maghemite nanoparticles for Pb (II) removal in aqueous solution. *J. Ind. Eng. Chem.* **2012**, *18*, 1582−1589.

(35) Wang, J.; Guo, X. Adsorption kinetic models: Physical meanings, applications, and solving methods. *J. Hazard. Mater.* **2020**, *390*, 122156.

(36) Sulaymon, A. H.; Mohammed, T. J.; Al-Najar, J. Equilibrium and kinetics studies of adsorption of heavy metals onto activated carbon. *Chem. Eng. Technol.* **2012**, *3*, 86−92.

(37) Köse, T. E.; Demiral, H.; Öztürk, N. Adsorption of boron from aqueous solutions using activated carbon prepared from olive bagasse. *Desalin. Water Treat.* **2011**, *29*, 110−118.

(38) Purkayastha, D.; Mishra, U.; Biswas, S. A comprehensive review on Cd (II) removal from aqueous solution. *J. Water Process Eng.* **2014**, *2*, 105−128.

(39) Hameed, B. H. Evaluation of papaya seeds as a novel non-conventional low-cost adsorbent for removal of methylene blue. *Chem. Eng. J.* **2009**, *162*, 939−944.

(40) Benhouria, A.; Islam, M. A.; Zaghouane-Boudiaf, H.; Boutahala, M.; Hameed, B. H. Calcium alginate−bentonite−activated carbon composite beads as highly effective adsorbent for methylene blue. *Chem. Eng. J.* **2015**, *270*, 621−630.

(41) Abid, M.; Niazi, N. K.; Bibi, I.; Farooqi, A.; Ok, Y. S.; Kunhikrishnan, A.; Ali, F.; Ali, S.; Igalavithana, A. D.; Arshad, M. Arsenic (V) biosorption by charred orange peel in aqueous environments. *Int. J. Phytorem.* **2016**, *18*, 442−449.

(42) Hassan, A. F.; Abdel-Mohsen, A. M.; Elhadidy, H. Adsorption of arsenic by activated carbon, calcium alginate and their composite beads. *Int. J. Biol. Macromol.* **2014**, *68*, 125−130.

(43) Uyar, G.; Kaygusuz, H.; Erim, F. B. Methylene blue removal by alginate−clay quasi-cryogel beads. *React. Funct. Polym.* **2016**, *106*, 1−7.

(44) Njimou, J. R.; Măicăneanu, A.; Indolean, C.; Nanseu-Njiki, C. P.; Ngameni, E. Removal of Cd (II) from synthetic wastewater by alginate−Ayous wood sawdust (Triplochiton scleroxylon) composite material. *Environ. Technol.* **2016**, *37*, 1369−1381.

(45) Roh, H.; Yu, M.-R.; Yakkala, K.; Koduru, J. R.; Yang, J.-K.; Chang, Y.-Y. Removal studies of Cd (II) and explosive compounds using buffalo weed biochar-alginate beads. *J. Ind. Eng. Chem.* **2015**, *26*, 226−233.

(46) Qin, L.; Yan, L.; Chen, J.; Liu, T.; Yu, H.; Du, B. Enhanced removal of Pb2+, Cu2+, and Cd2+ by amino-functionalized magnetite/kaolin clay. *Ind. Eng. Chem. Res.* **2016**, *55*, 7344−7354.

(47) Cai, C.-X.; Xu, J.; Deng, N.-F.; Dong, X.-W.; Tang, H.; Liang, Y.; Fan, X.-W.; Li, Y.-Z. A novel approach of utilization of the fungal conidia biomass to remove heavy metals from the aqueous solution through immobilization. *Sci. Rep.* **2016**, *6*, 36546.

(48) Yuan, P.; Fan, M.; Yang, D.; He, H.; Liu, D.; Yuan, A.; Zhu, J.; Chen, T. Montmorillonite-supported magnetite nanoparticles for the removal of hexavalent chromium [Cr (VI)] from aqueous solutions. *J. Hazard. Mater.* **2009**, *166*, 821−829.

(49) Chowdhury, S. R.; Yanful, E. K. Arsenic and chromium removal by mixed magnetite−maghemite nanoparticles and the effect of phosphate on removal. *J. Environ. Manage.* **2010**, *91*, 2238−2247.

(50) Gopalakannan, V.; Viswanathan, N. Synthesis of magnetic alginate hybrid beads for efficient chromium (VI) removal. *Int. J. Biol. Macromol.* **2015**, *72*, 862−867.

(51) Bajpai, J.; Shrivastava, R.; Bajpai, A. K. Dynamic and equilibrium studies on adsorption of Cr (VI) ions onto binary bio-polymeric beads of cross linked alginate and gelatin. *Colloids Surf., A* **2004**, *236*, 81−90.